ACS OMEGA

http://pubs.acs.org/journal/acsodf

Article

Design of Poly(cyclotriphosphazene)-Functionalized Zirconium Phosphate Nanoplatelets To Simultaneously Enhance the Dynamic Mechanical and Flame Retardancy Properties of Polyamide 6

Kuruma Malkappa,* Jayita Bandyopadhyay, and Suprakas Sinha Ray*

Cite This: *ACS Omega* 2020, 5, 13867−13877

Read Online

ACCESS | Metrics & More | Article Recommendations | Supporting Information

ABSTRACT: To obtain polyamide 6 (PA6) composites with improved flame retardancy and thermomechanical properties, highly cross-linked supramolecular poly(cyclotriphosphazene)-functionalized α-zirconium phosphate (f-ZrP) nanoplatelets were synthesized and melt-blended with PA6 in a twin-screw extruder. The performance enhancements of composites were investigated through measuring the dynamic mechanical property and observing cone calorimeter data, toxic gas evolution, and UL-94 rating. The thermomechanical performance of PA6 was increased by 37.2% after composite formation with f-ZrP. As for the fire retardancy performance, compared to neat PA6, the composite containing 10 wt % f-ZrP showed 41.7 and 30.4% decrease in the peak heat and total heat release rates, respectively, and the UL-94 rating of the composite was V-0. Moreover, the thermogravimetric analysis combined with infrared spectroscopy revealed that the addition of f-ZrP to the PA6 led to decrease in the evolution of the volatile compounds and toxic gases, with the formation of highly cross-linked P−N-containing dense char with microspheres, providing a strong barrier to the inhibition of the heat and flammable volatile components transferring between the flame zone area and substrate during the combustion test. Finally, based on the obtained results, the possible mechanisms for improved mechanical and fire retardancy properties of the composites were proposed.

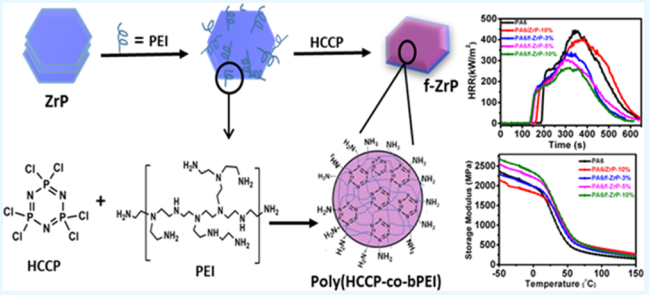

1. INTRODUCTION

In recent years, flame-retardant (FR) polymer composites with layered structured nanomaterials such as layered silicates,[1,2] layered double hydroxides,[3] graphite oxides,[4,5] layered metal oxides,[6−8] molybdenum sulfides,[9] and metal phosphate compounds[10] have been extensively studied, among which zirconium phosphate (ZrP)-layered nanomaterials have gained more attention regarding the progression of effective FRs for polymer composites.[11] For instance, ZrP contains unique advantages over MMT, such as an easy surface modification, a synthetic layered structure composed with metal Zr atoms, and phosphate groups, which are important to increase the FR activity.[12] Previous studies have confirmed that ZrP is a type of strong cross-linking catalyst because active Lewis acid sites are contained on the surface of each ZrP layer, which can accelerate the polymer degradation during the early stage of thermal oxidative degradation. Hence, ZrP is frequently used as an additive FR for polymers to improve the FR activity.[13] ZrP was first discovered by Clearfield and Stynes in 1964,[14] and in the structure of ZrP, it was confirmed that the Zr metal atoms are present on both sides of the layer midpoint, bonding to each oxygen atom of six different phosphate groups. Furthermore, three oxygen atoms of the phosphate group coordinate with three different Zr metal atoms, and the remaining oxygen atoms protonate to form a −OH group. In addition, α-ZrP is an inorganic compound, and it is difficult to uniformly disperse in a polymer matrix, resulting in a poor dispersion that clearly distorts the mechanical and flammability properties.[15] These hydroxyl groups are useful for further modification with suitable organic components, which can improve the FR activity and develop multifunctional hybrid nanofillers as an efficient FR for polymer composites.[16,17] Xie et al.[18] synthesized a novel macromolecular charring agent (MCA) functionalized on the surface of α-ZrP nanosheets and prepared polypropylene composites. They found that a composite with ZrP-d-MCA and ammonium polyphosphate (APP) of 5 and 15 wt % contents, respectively, exhibits a better FR activity and passes the V-0 rating in a UL-94 test because of the possible synergetic effect between the APP and FR compounds.

Polyamide 6 (PA6) is considered an important engineering plastic owing to its high demand in various advanced technologies and has been extensively used in automotive

Received: March 20, 2020
Accepted: May 19, 2020
Published: June 1, 2020

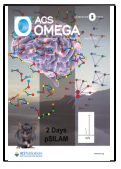

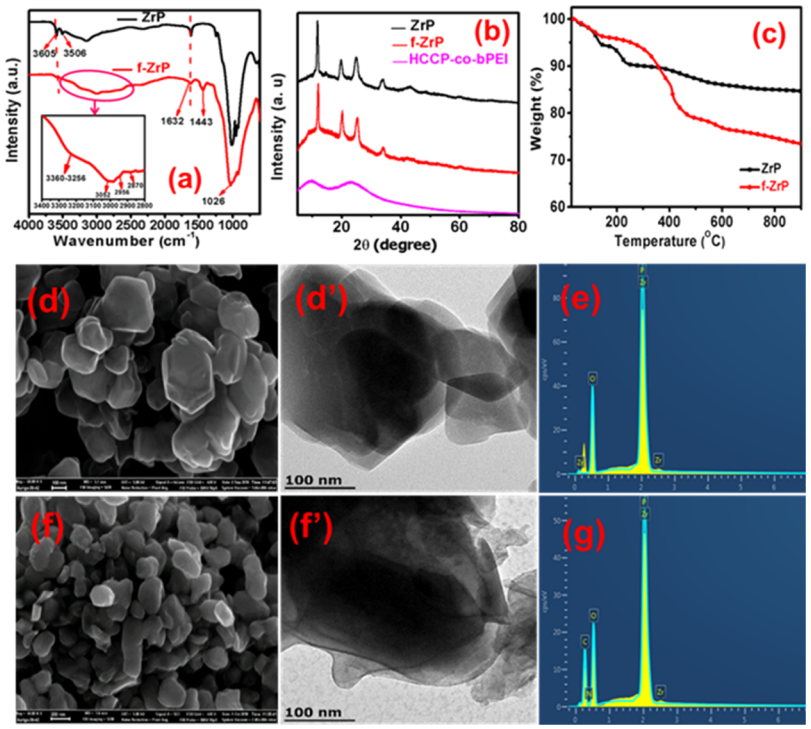

Figure 1. (a) FTIR spectra, (b) XRD patterns, and (c) thermogravimetric analysis of ZrP (α-ZrP) and f-ZrP. SEM images of (d) synthesized ZrP and (f) f-ZrP. Transmission electron microscopy images (d′) of synthesized ZrP and (f′) f-ZrP. EDX data of (e) synthesized ZrP and (g) f-ZrP.

production and the electric and electronic industries.[19,20] However, neat PA6 contains severe flammability and strong melt drippings during combustion and thus has limited structural applications.[21] Hence, it is important to improve the FR activity of PA6. Consequently, the improvement in the FR activity of PA6 has attracted numerous researchers in the last decade. Xiang et al.[22] used ZrP in combination with ammonium sulfamate (AS) to prepare PA6 composite fibers and measured flammability properties. They observed that the PA6 composite consists of 1.5 wt % of ZrP and 2 wt % of AS, showing a better FR activity and V-0 rating in the UL-94 test. Xu et al.[23] prepared a hybrid FR-reduced graphene oxide (rGO)@ZrP and further prepared EP composites, and the resulting EP/rGO@ZrP-2% composite showed an efficient FR activity because of a combination of properties such as physical barrier property of rGO and the catalysis effect of α-ZrP. Instead of blend FRs, to decrease the loading percentage in the polymer composites currently, synthesis of an effective hybrid FR in a suitable way for surface functionalization with other P-, N-, and P−N-containing compounds was initiated because it can improve the FR efficiency of the derived hybrid FR. Xing et al.[24] prepared organically modified ZrP (OZrP) and used it as a synergetic agent for PDHA-TGICA-PHEA coatings, and they observed that the composite system with 0.5 wt % of OZrP showed a significant decrease in heat release rate (HRR) and total heat release (THR) values. The melamine cyanurate-functionalized α-ZrP was synthesized using an *in situ* method, and a PA6 composite was prepared. It was observed that the composite with the 10 wt % α-ZrP@MCA content significantly decreased the HRR and THR and obtained a V-0 rating in the UL-94 test because of a combination effect of α-ZrP and MCA.[25]

Cyclotriphosphazene-derivative compounds are an important class of FR because they contain a controllable cyclic structure with alternate −P═N− units, resulting in high thermal stability and high limiting oxygen index (LOI).[26] The varieties of covalently cross-linked cyclotriphosphazenes can be synthesized using a normal precipitation method from hexachlorocyclotriphosphazenes (HCCPs) and low-molecular weight amines, alcohols, and thiol compounds, which are extensively used as adhesives and polymer additives in FRs.[27−30] Köhler et al.[31] synthesized highly cross-linked cyclomatrix polyphosphazene poly(HCCP-*co*-bPEI)s from HCCP and branched polyethylene imines (bPEI). They confirmed that the amine-terminated poly(cyclophosphazenes) obtained possess high thermal stability and high adhesion properties, which are more useful as additives in FRs used in polymer coatings. The most commonly used and promising method for developing an efficient FR is using nanofiller surface functionalization, in which the improvement in the FR property mainly depends on the choice of the nanofiller and surface modifier. Previous reports revealed that the different types of amine compounds utilized for APP surface modification, such as aliphatic diethylenetriamine (DETA),[32] cyclic piperazine (PAz),[33] and bPEI,[34] can be further used to prepare EP composites. The resulting EP composites exhibit a better FR activity with a significantly decreased HRR and smoke suppression, as compared to neat EP. However, bPEI showed a better FR activity than DETA and PAz because of the hyper bPEI structure, and it contains more reactive different types of amine functionalities such as primary, secondary, and ternary amines.

In this direction, we have chosen HCCP to react with bPEI for the surface modification of α-ZrP (from now ZrP) nanoplatelets, as described in the Experimental Section. During such preparation, the ZrP nanoplatelets act as a hard template and create a type of absorption and polymerization mechanism. The highly poly(HCCP-*co*-bPEI) formed is uniformly functionalized on the surface of the ZrP, and thus the organic/inorganic hybrid FR obtained is considered to be

https://dx.doi.org/10.1021/acsomega.0c01247
ACS Omega 2020, 5, 13867−13877

functionalized α-zirconium phosphate (f-ZrP). However, highly cross-linked hybrid FR f-ZrP-containing PA6 composites are yet to be reported. In this study, the hybrid FR f-ZrP contains cyclomatrix polyphosphazene poly(HCCP-*co*-bPEI) on the surface, which is useful to increase the interfacial interactions with the polymer matrix, resulting in an improvement of the thermomechanical and fire-retardant properties of the polymer composites. In this work, we report the use of PA6 composites with various amounts of newly derived hybrid FR f-ZrP and ZrP, and a thorough study was conducted on the thermal and FR properties.

2. RESULTS AND DISCUSSION

2.1. Formation of f-ZrP. To confirm the successful surface functionalization of ZrP, the Fourier transform infrared (FTIR) analysis was carried out, and the resulting spectra of α-ZrP and f-ZrP are presented in Figure 1a. Sharp peaks appeared at 3506 and 3605 cm^{-1} corresponding to stretching vibrations of P−OH. The broad peak at 3000−3500 and 1628 cm^{-1} corresponds to the lattice water. The absorption peak at 1308 is attributed to the $-PO_3$ stretching vibrations. The absorption bands at 925 and 630 cm^{-1} are attributed to the $-PO_3$ bending vibrations. In the case of f-ZrP, the characteristic peaks of P−OH at 3506 and 3605 cm^{-1} mainly disappeared,[35] which suggests that the hydrogen from P−OH was successfully replaced with $-NH_2$ of bPEI.[36] Typical peaks appearing at 867 and 1206 cm^{-1} are attributed to the −P−N− and −P═N−, respectively, which are characteristic absorption peaks of cyclotriphosphazene.[20,37] However, the main characteristic and broad peaks appearing at 3256−3360 cm^{-1} correspond to the amino group of bPEI. This clearly indicates the successful occurring of condensation reaction between bPEI and HCCP on the surface of ZrP.[30] Further, to confirm the surface modification of ZrP, the X-ray diffraction (XRD) analysis was carried out, and the resulting XRD patterns of ZrP, f-ZrP, and a poly(HCCP-*co*-bPEI) copolymer are presented in Figure 1b. It can be clearly seen in the case of pristine α-ZrP that the characteristic strong peaks appearing at 2θ = 11.58, 19.28, 25.53, and 34.09° correspond to the crystal faces of (002), (110), (112), and (215), respectively. All peaks show good agreement with earlier reports of ZrP.[35] For f-ZrP, there is no peak shifting, but the intensities of the peaks decreased compared to the pristine ZrP. This clearly shows that the amorphous poly(HCCP-*co*-bPEI)[31] is continuously functionalized on the surface of the ZrP nanoplatelets like a layer, resulting in weaker peak intensities.

Further, to identify the thermal stability and amount of poly(HCCP-*co*-bPEI) copolymer functionalized on the surface of the ZrP nanoplatelets, samples of ZrP and f-ZrP were applied to a thermogravimetric analysis, as shown in Figure 1c. The weight loss of ZrP at 900 °C was approximately 15.1% with a two-step thermal degradation. At approximately 100 °C, the first weight loss occurred owing to a complete dehydration of water. The second weight loss occurred mainly owing to the condensation of the phosphate groups of ZrP, which started at approximately 150−240 and 400−500 °C, resulting in complete dehydration and forming zirconium pyrophosphate.[38] Similarly, the char residues remaining at 900 °C for f-ZrP are 73.5%. Hence, the poly(HCCP-*co*-bPEI) functionalized on the surface of ZrP is 11.4%.

The morphologies of the synthesized ZrP and f-ZrP are also presented in Figure 1. The pristine ZrP exhibits a sheet-type morphology and a smooth surface, as shown in Figure 1d [scanning electron microscopy (SEM)] and d′ [transmission electron microscope (TEM)]. After modification with bPEI and HCCP, with an alternative addition to the α-ZrP-dispersed solution presented in the Experimental Section, a capsule-shaped morphology develops, as shown in Figure 1f (SEM) and f′ (TEM). Because the dissolved bPEI in acetonitrile was slowly added to the ZrP-dispersed solution during surface modification, it results in the formation of strong ionic interactions between $-NH_2$ groups of bPEI and the −OH group of ZrP; furthermore, the dissolved HCCP in acetonitrile was slowly added to the reaction mixture. The amine groups of bPEI further reacted with the chlorine of HCCP and formed a combined highly cross-linked P- and N-containing copolymer product defined as poly(HCCP-*co*-bPEI),[31] which was obtained through nucleophilic substitution and adheres to the surface of the ZrP nanoplatelets, spreading all over each sheet.[20] The energy-dispersive X-ray (EDX) data on ZrP and f-ZrP are shown in Figure 1e,d, respectively, and in the case of f-ZrP, the characteristic peaks of C and N elements were additionally observed, as shown in Figure 1g, which indicates that the poly(HCCP-*co*-bPEI) formed was successfully functionalized on the surface of the ZrP nanosheets. The above conclusions have been supported by the EDX elemental mapping data presented in Figure S1, Supporting Information.

2.2. Composite-Fractured Surface Morphology. To determine the possible interfacial interactions between f-ZrP and a PA6 polymer matrix, the freeze-fractured surface morphology of the PA6 composites was analyzed using field-emission SEM (FESEM), the resulting images of which are shown in Figure 2, because the interfacial interactions play the important role to improve the thermomechanical and

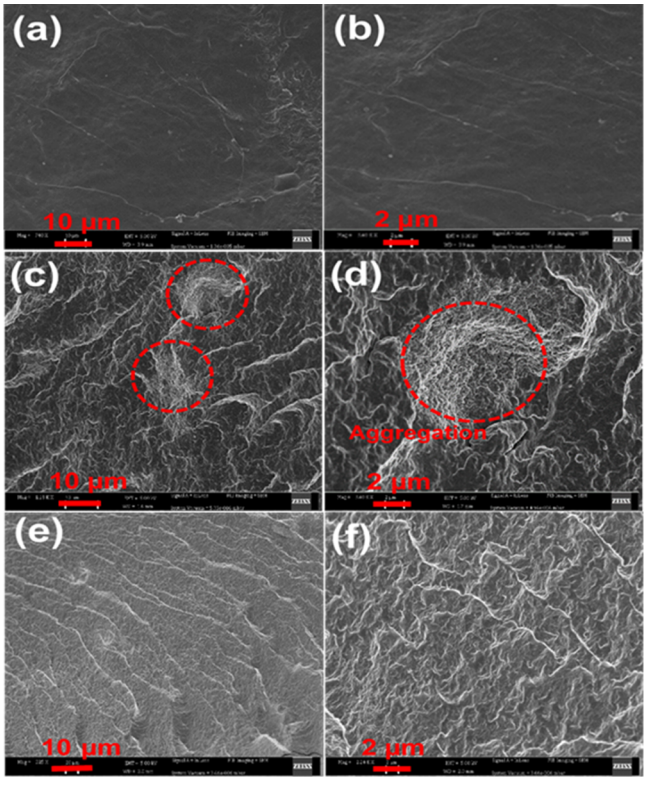

Figure 2. SEM of the fractured surface morphology of (a,b) neat PA6, (c,d) PA6/ZrP-10% composite, and (e,f) PA6/f-ZrP-10% composites with different magnifications.

https://dx.doi.org/10.1021/acsomega.0c01247
ACS Omega 2020, 5, 13867−13877

flammability performance of the polymer composites. The fractured surface morphology of the PA6 composites showed a much rougher surface than that of neat PA6, Figure 2a,b. After the addition of ZrP and f-ZrP to the PA6 polymer, the morphology of the composites showed a noticeable difference among neat PA6 and the PA6/ZrP-10% and PA6/f-ZrP-10% composites. The morphologies of the PA6/ZrP-10% composite, shown in Figure 2c,d, and the ZrP nanoplatelets are agglomerated. In Figure 2e,f, the PA6/f-ZrP-10% composite shows a wrinkled structure, and there are no scratches in the morphology. This indicates the possible strong interfacial interactions present between the $-NH_2$ group of f-ZrP nanofiller and the carbonyl groups of PA6 polymer matrix. Moreover, it can be seen that several f-ZrP nanoplatelets are embedded on the fractured surface of the PA6 polymer. This could be attributed to the surface modification with poly(HCCP-*co*-bPEI) present on the surface of the ZrP and the decreased polarity.[39,40] Hence, the improved compatibility between the f-ZrP and PA6 polymer matrix results in a uniform dispersion, thereby increasing the mechanical and flammability properties of the PA6 composites.

2.3. Dynamic Mechanical Analysis. The dynamic mechanical behavior of PA6 and its composites with f-ZrP were analyzed using a dynamic mechanical analyzer (DMA), which provides complete information related to the viscoelastic properties of a polymer matrix, showing changes in the mechanical stiffness and the relaxation process, as a function of temperature. The storage modulus (E') and tan δ plots of PA6 and its composites obtained through DMA are shown in Figure 3. It can be clearly seen from Figure 3a that the E' values

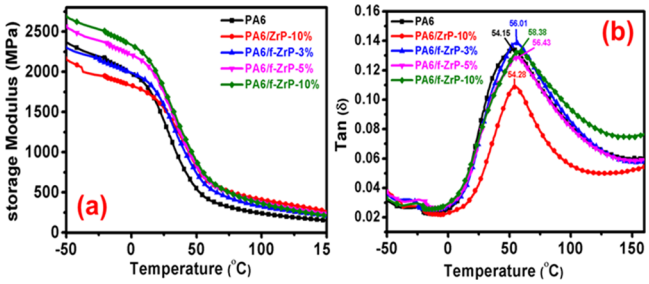

Figure 3. Dynamic mechanical analysis of PA6 and its composites with ZrP (α-ZrP) and f-ZrP under different percentages of loadings: (a) storage modulus and (b) tan δ.

increase for the PA6 composites with f-ZrP and decrease with the unmodified ZrP, as compared to that of the neat PA6. Owing to the surface of ZrP modified with a highly cross-linked poly(HCCP-*co*-bPEI) copolymer, which comprises a hyper-branched polyamine, the amine functionality on the surface of f-ZrP interacts with the carbonyl groups of PA6 polymer matrix and improves the interfacial interactions. Moreover, the E' values significantly increase with the increaseing f-ZrP content in the PA6 composites, owing to the reinforcing effect of the f-ZrP, and increase with the increasing f-ZrP content in the PA6 matrix. The E' value for the PA6/f-ZrP-10% composite is enhanced by over 37.2% compared to that of the neat PA6. In the case of unmodified ZrP-containing composites, the ZrP nanosheets are agglomerated, as observed in the fractured cross-section FESEM image shown in the previous section. This may be because of the lack of thermodynamically favorable interaction between the ZrP surfaces with the PA6 polymer matrix. On the other hand, the storage modulus of PA6 and its composites show a similar behavior at high-temperature regions and sharply decrease with an increase in the temperature with a levelling off at high-temperature regions. It is well known that this is because the polymer below the transition is glassy and above the transition temperature is rubbery.[41]

The tan δ plots are shown in Figure 3b, where all PA6 composites and the neat PA6 exhibit two clear peaks, called α and β transitions, at approximately 56 and −35 °C, respectively. The β transition observed at approximately −35 °C corresponds to the damping of the carbonyl group of PA6 involved in the formation of hydrogen bonds with absorbed water.[42−44] It can also be clearly seen from all tan δ plots that the position and intensity of the β transition peaks are not varied, which mainly depends on the water absorption.[45] The other α transition obtained with a high peak intensity at a higher temperature and is considered to be the glass transition temperature (T_g), and T_g of the neat PA6 is observed at 54.15 °C. Moreover, it can be found from the tan δ plots that the T_g values slightly increased to a higher temperature for all FR PA6/f-ZrP composites as compared to that of neat PA6. In addition, notice that with an increase in the f-ZrP content in the PA6 composites, the T_g values also slightly increased, which is ascribed to the strong interfacial interactions between the PA6 polymer chains and f-ZrP, and thus, restricting the polymer chain mobility results in increased T_g values. On the other hand, it can be found from the tan δ plots that the T_g value of PA6/ZrP-10% composite (54.28 °C) is almost the same as that of neat PA6 (54.16 °C). Such an observation again supports that there is no interfacial interaction between the ZrP particles and PA6 matrix.

2.4. Thermal Stability. The thermal stability and degradation behavior of PA6 and its composites with different percentages of ZrP and f-ZrP loadings were evaluated in the presence of N_2 and air, and the distinctive thermogravimetric analysis (TGA) curves are shown in Figure 4. The thermal stability of the composites quantified based on the initial degradation temperature (T_{deg}) at 5% weight loss, maximum degradation temperature (T_{max}) at 80% weight loss, and char

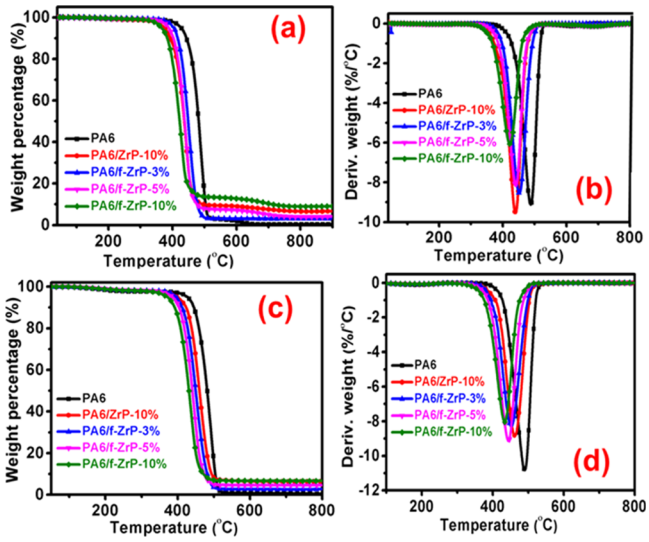

Figure 4. TGA and DTG curves of PA6 and its composites with different percentages of α-ZrP and f-ZrP as indicated under (a,b) nitrogen and (c,d) air.

https://dx.doi.org/10.1021/acsomega.0c01247
ACS Omega 2020, 5, 13867−13877

Table 1. TGA and DTG Data of all PA6 and Its Composite Samples with Different ZrP and f-ZrP Amounts in N_2 and under Air[a]

	N_2 atmosphere				O_2 atmosphere			
samples	T_{deg} (°C)	T_{max} (°C)	char at 800 °C (%)	α_{max} (%/°C)	T_{deg} (°C)	T_{max} (°C)	char at 800 °C (%)	α_{max} (%/°C)
PA6	423.8	498.6	0.3	−8.5	412.3	492.6	0.2	−11.4
PA6/ZrP-10%	386.7	479.1	5.3	−9.4	371.3	467.1	5.2	−8.7
PA6/f-ZrP-3%	402.6	470.7	3.4	−8.3	398.6	461.9	2.6	−8.0
PA6/f-ZrP-5%	389.7	459.0	4.1	−8.1	387.7	447.6	4.4	−9.0
PA6/f-ZrP-10%	372.5	448.4	10.5	−5.9	365.1	434.3	7.1	−7.8

[a] T_{deg}, temperature at 5% weight loss; T_{max}, temperature at 80% weight loss; α_{max} is the conversion corresponding to the maximum differential kinetic curve.

residue remains at 800 °C is listed in Table 1. From Figure 4, in both N_2 and air, the TGA curves of the PA6 composites typically display a one-stage decomposition similar to neat PA6, except in the earlier degradation of the polymer in the presence of f-ZrP. As clearly observed from Figure 4a and the data in Table 1, T_{deg} and T_{max} of the neat PA6 are approximately 423 and 498 °C, respectively. Although T_{deg} and T_{max} of the PA6 composites are further decreased to a different extent, this is because of the catalytic effect of f-ZrP, which contains Lewis solid acid sites on the surface, accelerating the earlier thermal degradation of the polymer. From Figure 4b, the derivative thermogravimetry (DTG) curves show obvious changes in T_{max} between the neat PA6 and PA6 composites, and with an increase in the f-ZrP content in the composites, the degradation rate is further depressed, as evidenced by the DTG plots. Because this accelerates the polymer degradation in the early stage and promotes the cross-linked reactions of the composite matrix to quickly form a strong char layer capable of protecting the underlined material from further degradation from higher temperatures, the results show an improved char residue. Hence, the char residue of the PA6/f-ZrP-10% composites shows a 10.5% higher char yield than neat PA6 (0.3%) and PA6/ZrP-10% composite (5.3%). This is mainly because of the catalysis effect of ZrP and the highly cross-linked poly(HCCP-*co*-bPEI) on the surface of ZrP facilitating the char formation and char structure during thermal degradation. The TGA plots of PA6 and its composites under air are shown in Figure 4c,d and Table 1. Similar results are found under air as under nitrogen, although T_{deg} and T_{max} of all samples are slightly decreased. Moreover, compared to under nitrogen, the presence of oxygen relatively decreased the char residues, which might be because of the combined effects between oxygen and temperature being more adverse to the formation of stable char at high temperature.

2.5. Analysis of Released Pyrolytic Gaseous Components of PA6 and Its Composites Using TG-FTIR. TG-FTIR is an important technique with the ability to track the released pyrolysis gas components during the thermal degradation process. The released pyrolysis gases are qualitatively and semi-quantitatively analyzed based on the infrared characteristic peak position and absorbance intensities of their characteristic peak intensity in the infrared spectra.[46,47] The FTIR spectra of all formulated gaseous components of PA6 and the PA6/f-ZrP-10% composite at maximum degradation rates are shown in Figure 5a. Based on the FTIR peak signals, the typical decomposed gaseous components are remarkably identified along with the characteristic absorption peaks, such as those of the amine groups (3500−4000 cm^{-1}), CO_2 (2360 cm^{-1}), CO (2130 cm^{-1}), −C═O group of carbonyl compounds (1740 cm^{-1}), and −C−H group

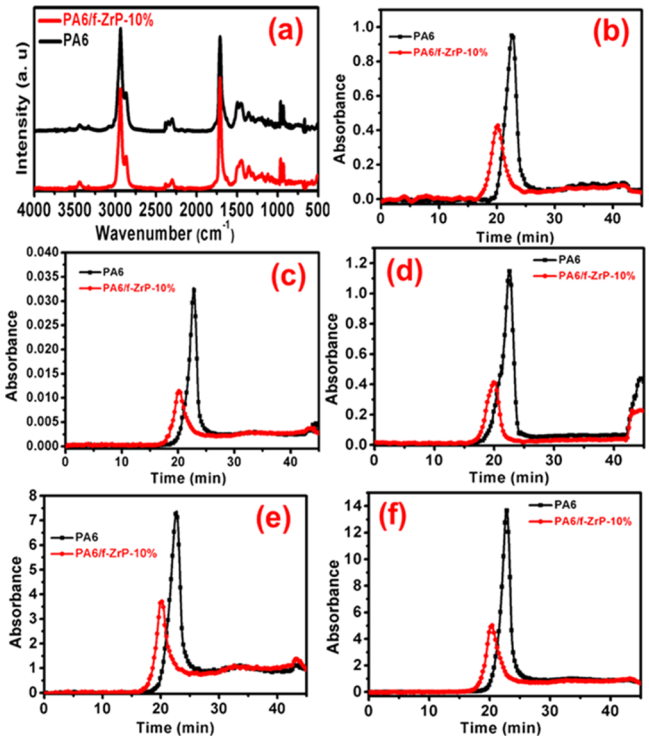

Figure 5. TGA−FTIR spectral plots of released volatile components for PA6 and PA6/f-ZrP-10%: (a) FTIR spectra, (b) Grams−Schmidt curves, (c) CO, (d) CO_2, (e) carbonyl, and (f) hydrocarbons.

of hydrocarbons (2800−2900 cm^{-1}). It can be clearly seen from the FTIR spectra that the thermal degradation path of the PA6/f-ZrP-10% composite is the same as that of the neat PA6, which means that the f-ZrP does not have much influence on the thermal degradation path but accelerates the polymer degradation faster, forming a strong thermal-insulating char. In addition, the effect of f-ZrP on the pyrolysis process of the PA6 composites was investigated, and to understand the released pyrolysis compounds, the absorbance intensity of the total volatile components (Gram−Schmidt curves), CO, CO_2, carbonyl compounds, and hydrocarbons versus the time curves is shown in Figure 5b−f. The Gram−Schmidt curve is presented in Figure 5b, which reveals the complete FTIR absorbance intensity of the total released pyrolytic gaseous components over the recorded wavenumber range (600−4000 cm^{-1}) in each weight loss occurring during thermal degradation. It can clearly be seen that it exhibits a sharp peak in both cases, which corresponds to the maximum weight loss occurring in the TGA. Sharp peaks of the PA6 and PA6/f-ZrP-10% composites appeared at approximately 21.94 and

https://dx.doi.org/10.1021/acsomega.0c01247
ACS Omega 2020, 5, 13867−13877

20.13 min, respectively. The heating rate of the sample run is 20 °C/min, and thus the corresponding peak temperatures can be expected in a TGA furnace at 438.8 and 402.6 °C. This clearly reveals that the vigorous degradation process of the PA6/f-ZrP-10% composite will be faster compared to that of the neat PA6. Hence, the presence of f-ZrP accelerates the polymer degradation faster, resulting in the peak of the Gram−Schmidt curves shifting to a lower side, which might be attributed to the earlier detection of the evolved pyrolytic gases compared to that of the neat PA6. It should also be noted that these similar observations of the peak shifts in the DTG curves are related to T_{max} of PA6 and the PA6/f-ZrP-10% composite shown in Figure 5b,d. However, the total absorbance intensity of the PA6/f-ZrP-10% composite is significantly reduced, implying that it suppresses the release of the pyrolytic gas components. This is because the ZrP accelerates the polymer degradation to form char at an earlier stage, and the poly(HCCP-*co*-bPEI) on the surface further involves the formation of cross-linked P−N-containing compounds during the thermal degradation and is retained in the char, making it stronger. Hence, it contributes to the better barrier properties, inhibiting the toxic gas evolution and small organic components, which are responsible for the increase in the fire-risk properties. Moreover, the absorption intensity versus time plots of various types of volatile gases in PA6/f-ZrP-10% are also highly inhibited, as shown in Figure 5c−f, including CO_2 (2310 cm^{-1}), CO (2100 cm^{-1}), carbonyl compounds (1736 cm^{-1}), and hydrocarbons (2800−2900 cm^{-1}). The decrease in the pyrolytic gases and hydrocarbons indicates a decrease in the HRR values, as observed in the cone calorimeter test results discussed in the next session. It is well known that volatile organic components easily crack into small hydrocarbons and further condense to form smoke particles, which can reduce the visibility and act as a fuel to support continual combustion.[48] Hence, the presence of f-ZrP obviously decreases the pyrolytic hydrocarbons, thus increasing the fire safety of PA6.

2.6. Analysis of Flammability, Smoke, and Toxic Smoke Production Properties of PA6 Composites. A cone calorimetry test is an effective tool to analyze the flammability of the materials because it can simulate the polymer materials under real combustion conditions. To evaluate the effects of ZrP and f-ZrP on the flammability properties of PA6, a cone calorimetry test was carried out in this study. All derived plots as a function of time from the cone calorimetry test are shown in Figure 6, and data are listed in Table 2. The peak HRR ($_p$HRR) and THR are important parameters to evaluate the flame retardancy, and these lower values are an indication for a high flame retardancy. The $_p$HRR and THR curves of PA6 and its composites with α-ZrP and f-ZrP are presented in Figure 6. The PA6 burns easily, and after complete ignition of pristine PA6, $_p$HRR and THR values of 443.8 kW m^{-2} and 118.2 MJ m^{-2} were observed, respectively. Figure 6 clearly shows that after the introduction of ZrP and f-ZrP into the PA6 matrix, the resulting PA6 composites show relatively decreased $_p$HRR and THR values compared to the neat PA6. This is because the ZrP acts as a strong cross-linked catalyst and accelerates the polymer degradation during the early stage, which is consistent with the TGA results. Compared to the neat PA6, the $_p$HRR and THR values of the PA6/ZrP-10% composite slightly decreased to 398.6 kW m^{-2} and 111.4 MJ m^{-2}, respectively. This is mainly because of the acid catalytic effect of ZrP, which accelerates the polymer degradation during the early stage to form a thermal-insulating char that can inhibit the heat and mass transformations. For the PA6/f-ZrP-3% composites, the $_p$HRR and THR values are 338.1 kW m^{-2} and 90.4 MJ m^{-2}, respectively. However, in the PA6 composite with the increasing f-ZrP content, the $_p$HRR and THR values further decreased, and in the PA6/f-ZrP-10% composite, the $_p$HRR and THR values are 258.5 kW m^{-2} and 82.2 MJ m^{-2}, respectively. Compared to the neat PA6, the $_p$HRR and THR values of the PA6/f-ZrP-10% composite are significantly reduced by 41.75 and 30.45%, respectively.

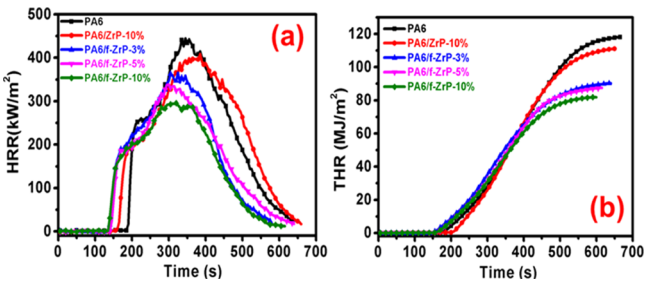

Figure 6. (a) HRR and (b) THR plots of PA6 and its composites with α-ZrP and f-ZrP under different weight percentages as indicated in the figure.

Moreover, in the UL-94 test, only the PA6/f-ZrP-10% composite sample exhibited V-0 rating, which is an ideal rating for FR application. The digital pictures, presented in Figure 7, captured the state of burning during UL-94 tests. In Figure 7a, once the neat PA6 was ignited, the flame developed bigger and bigger, and after 21 s, it self-extinguished through melt-dripping. This situation was improved in the case of PA6/f-ZrP-5% composite; the flame was self-extinguished within 5 s without melt-dripping, Figure 7b. However, the superior result was observed in the case of PA6/f-ZrP-10% composite, where the flame was self-extinguished within 5 s with the highest integrity of the structure.

This is because the α-ZrP modified with poly(HCCP-*co*-bPEI) results in the ZrP acting as an acid catalyst degrading the polymer during the early stage, and the surface contains hyper-branched polyamines containing a poly(HCCP-*co*-bPEI) copolymer. It can increase the cross-linked compound formation with degraded components of PA6, which are present in char and improve the char structure. Therefore, it can form a highly cross-linked P−N-containing char structure that provides strong barrier properties to inhibit the heat and mass transfers.

The release of smoke and toxic gases is the main parameter when estimating the risk of polymer materials during combustion. Figure 8 shows the carbon dioxide production (CO_2P), carbon monoxide production (COP), total smoke production (TSP), and total smoke release (TSR) plots of the PA6 and its composites. In addition, the specified values are listed in Table 2. The CO_2P and COP curves of PA6 and its composites are shown in Figure 8a,b. In general, cone calorimetry operates on the oxygen consumption principle. Therefore, the releasing HRR values of the burning polymer and its composites are equivalent to those of the oxygen consumption. During the polymer combustion and simultaneous release of heat radiation, some other oxidized gases and CO_2 also occur. Hence, the CO_2 plots of PA6 and its composites exhibit shapes similar to those in the HRR plots shown in Figure 6a. The neat PA6 shows a higher COP and

https://dx.doi.org/10.1021/acsomega.0c01247
ACS Omega 2020, 5, 13867−13877

Table 2. Cone Calorimetry Data of PA6 and Its Composites with Different Weight Percentages of ZrP and f-ZrP Obtained from the Flammability Test[a]

sample	$_{p}$HRR (kW m^{-2})	TTI (s)	$t_{_{p}HRR}$ (s)	THR (MJ m^{-2})	FGI (kW m^{-2}·s^{-1})	COP (mg/s)	CO_2P (mg/s)	TSP (m^2/kg)	TSR (m^2/m^2)	t_1/t_2	melt dripping	UL-94 rating
PA6	443.8	183.8	336	118.2	1.32	3.9	326	4.36	434	24/-	Y	NR
PA6/ZrP-10%	398.6	155.4	372	111.4	1.07	3.6	262	3.72	373	11/8	Y	NR
PA6/f-ZrP-3%	338.1	134.6	319	90.4	1.02	3.3	241	2.52	254	7/6	N	V-2
PA6/f-ZrP-5%	301.3	140.5	305	87.3	0.94	3.1	243	2.10	230	6/5	N	V-2
PA6/f-ZrP-10%	258.5	132.5	311	82.2	0.81	2.5	217	2.06	209	3/2	N	V-0

[a] $_{p}$HRR, peak heat release rate; TTI, time to ignition; THR, total heat release; TSR, total smoke release; FGI, fire growth index (FGI = $_{p}$HRR/t_{pHRR}); t_1, application of 1st 10 s flame; t_2, application of 2nd 10 s flame; NR, no rating.

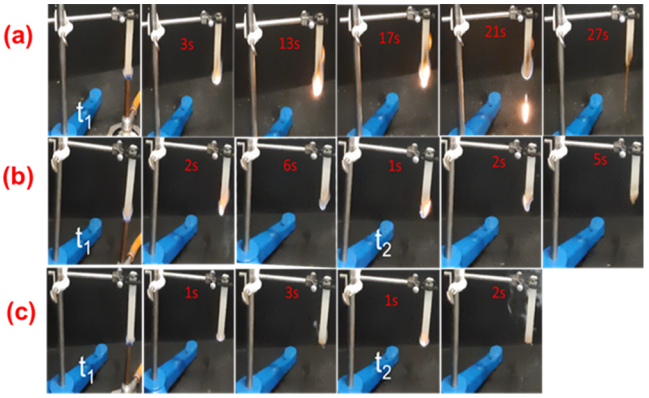

Figure 7. State of burning of (a) neat PA6, (b) PA6/f-ZrP-5%, and (c) PA6/f-ZrP-10% composite during the UL-94 test. The digital pictures reported in this figure were taken by K.M. who is the first author of this work.

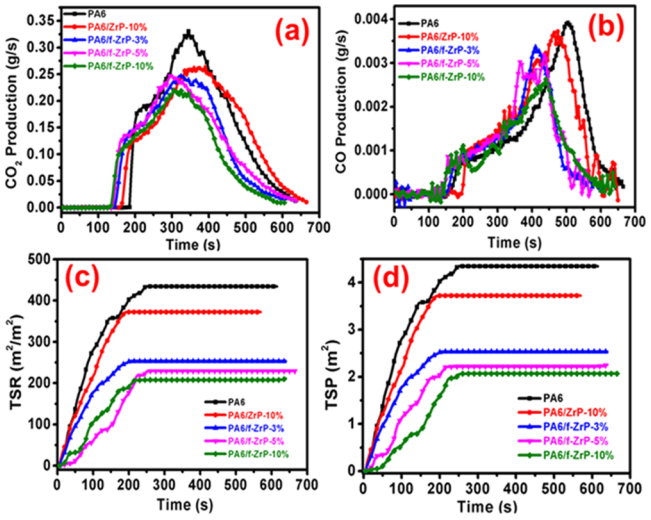

Figure 8. (a) CO_2P, (b) COP, (c) TSR, and (d) TSP plots of PA6 and its composites with ZrP and f-ZrP with different weight percentages, as indicated in figures.

CO_2P compared to the composites with ZrP and f-ZrP. However, in f-ZrP-containing PA6 composites, they decreased significantly, and with an increasing f-ZrP content, they decreased further. As shown in Table 2, the values of COP and CO_2P for the PA6/f-ZrP-10% composite are reduced by 35.89 and 33.45%, respectively. It can clearly be seen that the evolution of toxic gases is highly decreased with the modified ZrP FR. Figure 8c,d clearly indicates that the TSR and TSP of neat PA6 are larger, and the values of TSR and TSP are 434 m^2/m^2 and 4.36 m^2/kg, respectively. However, a large decrease occurred in the case of the PA6/f-ZrP-10% composite as compared to the pristine PA6, in which the values of the TSR and TSP are 209 m^2/m^2 and 2.06 m^2/kg, and the percentages of reduction are 51.84 and 52.75%, respectively. These indicate that the f-ZrP has a better smoke-suppressing characteristic than ZrP. This is because the surface modifier in the presence of f-ZrP can improve the char structure formation during combustion and make it stronger with the formation of a highly cross-linked P−N-containing char. In contrast, the f-ZrP in the composite is uniformly dispersed and has better physical barrier properties than ZrP. This is because ZrP is modified with a highly cross-linked P−N-containing poly(HCCP-*co*-bPEI) copolymer, which can interact with the PA6 polymer, resulting in the f-ZrP being uniformly distributed in the PA6 polymer. Based on the above analysis, a significant reduction in the toxic gases CO and CO_2 and the smoke production was observed in the presence of f-ZrP-containing composites, which is beneficial to lowering the fire risk and fire-related toxic gas release. The fire growth index (FGI) obtained from the cone calorimetry test results can be defined as the ratio of $_{p}$HRR value to the time to $_{p}$HRR. The FGI values are an indication of the flame spread rate, and as shown in Table 2, the FGI value for neat PA6 is 1.32 kW m^{-2} s^{-1}. However, the FGI value for the PA6 composites decreases, and the FGI value for the PA6/f-ZrP-10% composite is 0.81 kW m^{-2} s^{-1}, which is significantly decreased. Hence, the PA6/f-ZrP-10% composite exhibits a better fire-retardant activity.

2.7. Char Residue Analysis of PA6 and Its Composites with ZrP and f-ZrP. To analyze the FR mechanism, digital photographs of the residual char after the cone calorimetry test are shown in Figure 9. The neat PA6 burns strongly, and there are pieces of beaked char residue, as observed in Figure 9a, owing to the inferior char quality, and the inability to form an effective char layer to protect the underlying polymer material from further higher temperature degradation during combustion. The PA6 composite with α-ZrP shows an improved char residue compared to the neat PA6 polymer, shown in Figure 9b. However, the char has a loose structure and is broken because the char layer cannot expand at higher temperature. This indicates that the presence of ZrP increases the char residue owing to ZrP acting as a strong acid-catalyzing agent accelerating the polymer degradation and forming a thermal-insulating char earlier. However, the char cannot expand at higher temperature, resulting in a beaked char layer. However, the presence of f-ZrP-containing PA6 composites significantly increased the char residue with greater compactness and uniformly covered all areas, as shown in Figure 9c. Therefore, this indicates that the cooperation of the ZrP and highly cross-linked P−N-containing poly(HCCP-*co*-bPEI) polymer can

https://dx.doi.org/10.1021/acsomega.0c01247
ACS Omega 2020, 5, 13867−13877

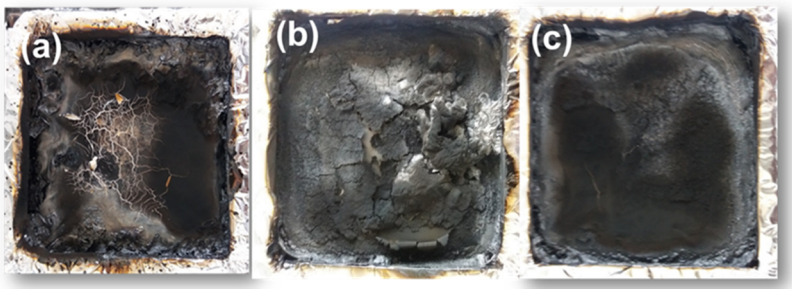

Figure 9. Digital photographs of residual char obtained from the cone calorimetry test: (a) pristine PA6, (b) PA6/ZrP-10%, and (c) PA6/f-ZrP-10% composites. The digital pictures reported in this figure were taken by K.M. who is the first author of this work.

improve the residual char compactness and char structure, which is helpful in increasing the FR activity of the PA6/f-ZrP composites.

Based on the above analysis, the addition of f-ZrP into the PA6 polymer matrix can improve the FR activity by suppressing the smoke and toxic gases during combustion. To complete the analysis of the FR mechanism, FESEM images of the char residues from cone calorimetry were recorded, as also shown in Figure 10. From Figure 10a,b, it

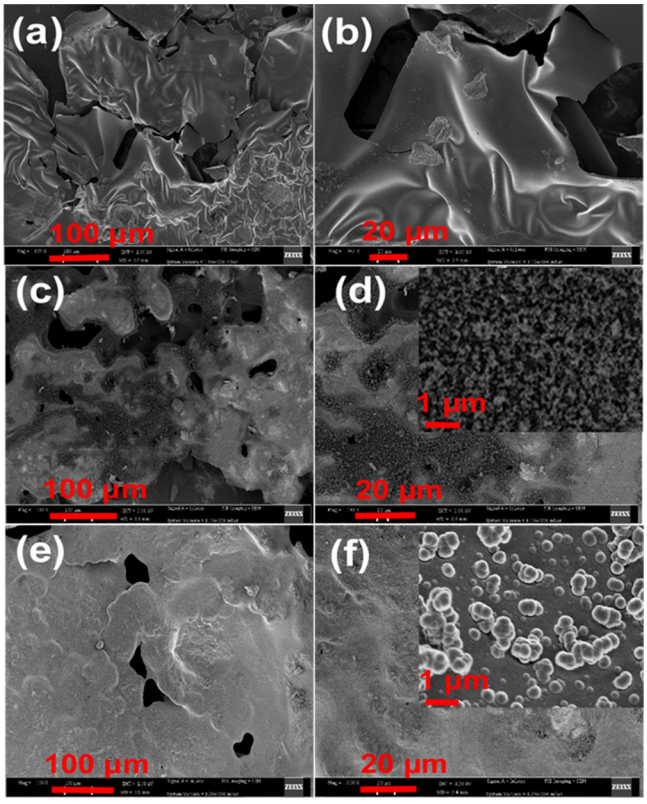

Figure 10. SEM images of residual char after the cone calorimetry test: (a,b) PA6, (c,d), PA6/α-ZrP-10 wt %, and (e,f) PA6/f-ZrP-10 wt % composites with different magnifications.

clearly shows that the neat PA6 burned out, and the resulting char residue seems like fluffy and broken char. The morphology of the PA6/α-ZrP-10% composite is shown in Figure 10c,d, and it forms a more porous structure with holes, indicating that the normal α-ZrP-containing PA6 composite system cannot achieve a better FR activity. However, the char morphology of the PA6/f-ZrP-10% composites shown in Figure 10e,f clearly indicates that a highly compact and continuous dense char is formed. Notably, the PA6 polymer matrix can decompose into small organic species with the catalytic action of the surface-modified poly(cyclotriphospazene) moiety shell part of f-ZrP, and degraded small organic components might be observed on the surface of the ZrP and continuously spread to form microspheres of char, as shown in the inset image in Figure 10f, which are retained in the char layer, resulting in a more compact and dense char.[49,50] This is efficient for decreasing the volatile organics and toxic gases, thereby improving the fire rescue properties. This phenomenon could not be observed in the case of the PA6/ZrP-10 composite, as shown in the inset image in Figure 10e. Therefore, it can act as a strong barrier to the inhibition of the heat and flammable volatile components transferring between the flame zone area and substrate during the combustion test. Hence, it improved the FR activity while protecting the underlined materials from further degradation and burning.

3. CONCLUSIONS

In this study, we synthesized inorganic ZrP (α-ZrP) nanoplatelets modified using a type of highly poly(HCCP-*co*-bPEI) through a coprecipitation method. First, modification with hyper bPEI was applied, followed by HCCP. All amine groups of bPEI react with chlorines of HCCP through nucleophilic substitution to form a highly cross-linked supramolecular type of polymer on the surface of the ZrP nanoplatelets, which is called a hybrid FR f-ZrP. A thermomechanical analysis revealed that, in the presence of f-ZrP, the PA6 composite storage modulus increased, and with an increased loading of the f-ZrP content in the PA6 composites, it further increased but decreased in the case of ZrP-containing PA6 composites. Because of the surface modification, the highly cross-linked polyphosphazenes present on the surface of ZrP nanoplatelets can help achieve a uniform distribution into the PA6 polymer matrix and improve the thermomechanical property including glass transition temperature. The TG-FTIR confirmed that, in the presence of f-ZrP, the PA6 composites significantly decreased the toxic gases and pyrolytic component evolution, and with increasing f-ZrP content in the PA6 composites, they further decreased. This is because it accelerates the polymer degradation during an earlier stage to form a thermal-insulating char. In PA6/f-ZrP-containing composites, the surface modification plays an important role in the formation of highly cross-linked microspheres of dense char with degraded components of the PA6 polymer, which can provide strong barrier properties, thus decreasing the amount of toxic gases and the heat evaluation. From a cone calorimetry analysis, the presence of f-ZrP-containing PA6 composites significantly

https://dx.doi.org/10.1021/acsomega.0c01247
ACS Omega 2020, 5, 13867−13877

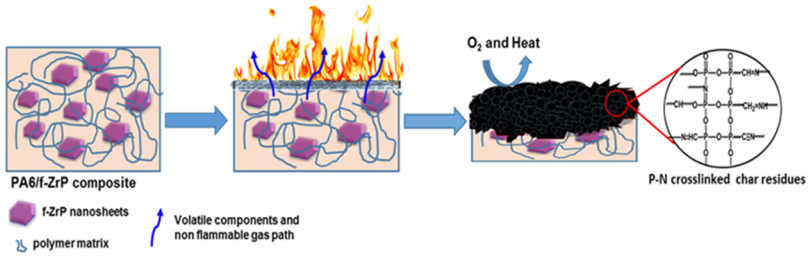

Figure 11. Proposed mechanism to explain the FR activity of PA6/f-ZrP composite.

decreased the evolution of the heat and toxic smoke, as compared to the neat PA6 and its composites with ZrP. This is because the surface of the ZrP contains highly cross-linked supramolecular poly(cyclotriphosphazenes) improving the char structure with the formation of char microspheres (Figure 11). During combustion, the surface modifier supramolecular poly(cyclotriphosphazenes) interact with the PA6 degradation components and form more cross-linked P−N-containing char microspheres that are present in char and become more compact, providing strong barrier properties to inhibit the heat and mass transfers. Hence, surface-functionalized α-ZrP is an efficient fire-retardant for a PA6 polymer in terms of decreasing fire risk and toxic smoke.

4. EXPERIMENTAL SECTION

4.1. Materials. PA6 (Commercial grade 1030B) with a melt flow index of 4.6 ± 0.23 g/10 min (at 250 °C under a 2.16 kg load), a weight average molecular weight of 30 kg/mol, a density of 1.14 g/cm^3, and a melting point of 220 °C, was obtained from UBE Industries Ltd., Tokyo, Japan. Zirconium oxychloride ($ZrOCl_2 \cdot 8H_2O$), acetonitrile, bPEI, HCCP, and phosphoric acid (98%) were purchased from Sigma-Aldrich, Johannesburg, South Africa and used as received without purification.

4.2. Preparation of α-Zirconium Phosphate (ZrP). α-ZrP was prepared through a refluxing method, according to previously reported studies.[35] The detailed procedure is as follows: 4 g of $ZrOCl_2 \cdot 8H_2O$ was taken into a round bottom flask, and 40 mL of 12 M phosphoric acid was added. Then, the reaction mixture was stirred for 24 h at 100 °C. After this, the resulting product α-ZrP was centrifuged and washed with deionized water and ethanol twice, and the compound obtained was then dried in an oven at 80 °C for 24 h.

4.3. Functionalization of α-ZrP (f-ZrP). First, 4 g of synthesized α-ZrP nanoplatelets (Figure 12a) was dispersed in 100 mL of acetonitrile and stirred for 30 min at 80 °C, and 1.6 g of bPEI dissolved in 40 mL of acetonitrile was separately and slowly added to the reaction mixture under stirring. Next, 4 mL of triethyl amine was added, and stirring was continued for another 2 h. Then, 0.76 g of HCCP was dissolved separately in 40 mL acetonitrile and added to the reaction mixture slowly over 30 min. The resulting reaction mixture was then sonicated for 3 h at a constant temperature of 60 °C. Next, the reaction mixture was centrifuged and washed with water and ethanol twice. The final product obtained was abbreviated as f-ZrP and dried in an oven at 80 °C for 24 h. The surface modification of α-ZrP with highly cross-linked poly(HCCP-*co*-bPEI) is presented in Figure 12b.

4.4. α-ZrP- and f-ZrP-Containing PA6 Composite Processing. The PA6 composites were prepared using a melt-blending process method with various weight percentages

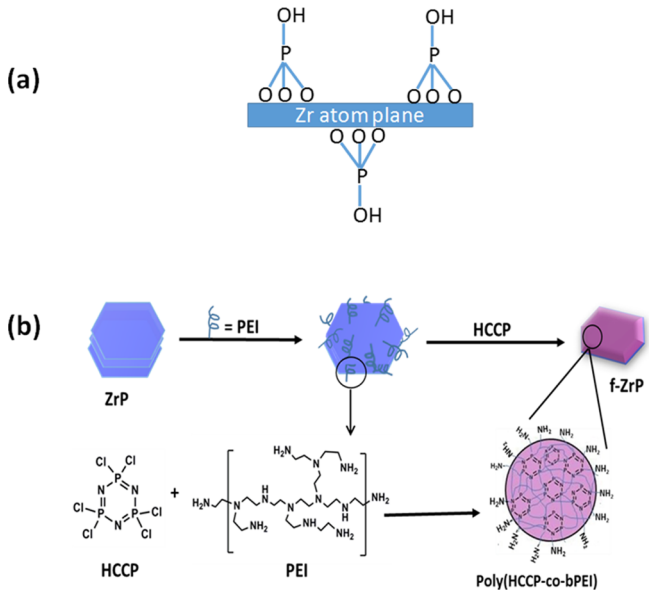

Figure 12. (a) Schematic of molecular structure of α-ZrP nanosheet and (b) schematic model for surface modification of α-ZrP with highly cross-linked poly(HCCP-*co*-bPEI).

of α-ZrP and f-ZrP. Before extrusion, all samples were dried in an oven overnight at 80 °C. During this processing, we used a twin-screw extruder (process 11, corotating twin-screw extruder, L/D = 40, Thermo Scientific, USA), and the extruded samples were collected using a water bath and pelletized. During the processing, we maintained different temperatures at different zones, such as 128, 240, 250, 260, 260, 260, and 260, and the die temperature was set to 250 °C, the screw speed was 200 rpm, and the samples obtained in the extruder were used for melt blending and compression molding at 240 °C for further analysis. All compression-molded (Carver, model 973214A, Wabash, USA) samples were first melted at 240 °C for 6 min, and a pressure of 9 MPa was applied for 1 min. Next, the molded samples were cooled down to room temperature using tap water, and the pressure was released. The samples obtained were then used for further characterization.

4.5. Characterization and Property Measurements. The FTIR spectra of the samples were obtained using a PerkinElmer FTIR spectrometer (Spectrum 100) in transmission mode, at a wavelength range of 600−4000 cm^{-1}, and all spectra of the 16 scans were collected at a resolution of 4 cm^{-1}. The XRD patterns of all synthesized powder samples, α-ZrP, f-ZrP, and poly(HCCP-*co*-bPEI), were collected from the X-ray generator using a PANalytical X'Pert PRO diffractometer (The Netherlands) and Cu Kα radiation (λ = 0.154 nm, current = 30 mA, and voltage = 40 kV). The diffractograms

https://dx.doi.org/10.1021/acsomega.0c01247
ACS Omega 2020, 5, 13867−13877

were collected at a scan rate of 0.6/min within the 2θ range 2−80°. The thermal stability and released degradable volatile components from PA6 and its composites with ZrP and f-ZrP at different weight percentages were evaluated using a hyphenated TGA−FTIR system, a PerkinElmer (USA) Pyris 1 TGA thermogravimetric analyzer connected to a Nicolet IS50 spectrometer within the temperature range of 50 to 800 °C, at a heating rate of 20 °C/min, under nitrogen. The weight of each tested sample was approximately 20 mg. The thermomechanical properties of PA6 and its composite compression-molded samples (dimensions of 13 × 6 × 2 mm^3) were evaluated using DMA(PerkinElmer 8000) in single bending mode, and at a temperature range of between −50 and 150 °C and with a temperature scan of 2 °C min^{-1} at 1 Hz frequency and a strain amplitude of 0.05%. The flammability properties of the PA6 and its composites with ZrP and f-ZrP at different weight percentages were studied using cone calorimetry (Fire Testing Technology, East Grinstead, UK), according to ISO 5660. The test samples prepared (dimensions of 100 × 100 × 3 mm^3) were wrapped in aluminum foil with the top surface open and exposed to a radiant cone at a heat flux of 25 kW m^{-2}. The microstructures of the char residues obtained from the cone calorimetry test were elucidated using SEM (AURIGA Crossbeam workstation, Carl Zeiss, Germany) at 3 kV.

■ ASSOCIATED CONTENT

Supporting Information

The Supporting Information is available free of charge at https://pubs.acs.org/doi/10.1021/acsomega.0c01247.

STEM−HAADF image and EDS mapping of f-ZrP (PDF)

■ AUTHOR INFORMATION

Corresponding Authors

Kuruma Malkappa − *Centre for Nanostructures and Advanced Materials, DSI-CSIR Nanotechnology Innovation Centre, Council for Scientific and Industrial Research, Pretoria 0001, South Africa*; Email: mkuruma@csir.co.za

Suprakas Sinha Ray − *Centre for Nanostructures and Advanced Materials, DSI-CSIR Nanotechnology Innovation Centre, Council for Scientific and Industrial Research, Pretoria 0001, South Africa; Department of Chemical Sciences, University of Johannesburg, Johannesburg 2028, South Africa;* orcid.org/0000-0002-0007-2595; Email: rsuprakas@csir.co.za, ssinharay@uj.ac.za, suprakas73@yahoo.com

Author

Jayita Bandyopadhyay − *Centre for Nanostructures and Advanced Materials, DSI-CSIR Nanotechnology Innovation Centre, Council for Scientific and Industrial Research, Pretoria 0001, South Africa*

Complete contact information is available at: https://pubs.acs.org/10.1021/acsomega.0c01247

Notes

The authors declare no competing financial interest.

■ ACKNOWLEDGMENTS

The authors would like to thank the Council for Scientific and Industrial Research (HGER74p) and Department of Science and Technology (HGERA8x) for financial support. The authors also thank Dr. Vincent Ojijo and Lesego Maubane for their help in the flammability tests and TG-FTIR analyses.

■ REFERENCES

(1) Fang, K.; Li, J.; Ke, C.; Zhu, Q.; Tao, K.; Zhu, J.; Yan, Q. Intumescent flame retardation of melamine-modified montmorillonite on polyamide 6: Enhancement of condense phase and flame retardance. *Polym. Eng. Sci.* **2011**, *51*, 377−385.

(2) Malkappa, K.; Bandyopadhyay, J.; Ray, S. Thermal degradation characteristic and flame retardancy of polylactide-based nano-biocomposites. *Molecules* **2018**, *23*, 2648.

(3) Nagendra, B.; Rosely, C. V. S.; Leuteritz, A.; Reuter, U.; Gowd, E. B. Polypropylene/layered double hydroxide nanocomposites: Influence of LDH intralayer metal constituents on the properties of polypropylene. *ACS Omega* **2017**, *2*, 20−31.

(4) Xu, W.; Liu, L.; Zhang, B.; Hu, Y.; Xu, B. Effect of molybdenum trioxide-loaded graphene and cuprous oxide-loaded graphene on flame retardancy and smoke suppression of polyurethane elastomer. *Ind. Eng. Chem. Res.* **2016**, *55*, 4930−4941.

(5) Xu, W.; Wang, X.; Wu, Y.; Li, W.; Chen, C. Functionalized graphene with Co-ZIF adsorbed borate ions as an effective flame retardant and smoke suppression agent for epoxy resin. *J. Hazard. Mater.* **2019**, *363*, 138−151.

(6) Wang, X.; Pang, H.; Chen, W.; Lin, Y.; Zong, L.; Ning, G. Controllable fabrication of zinc borate hierarchical nanostructure on brucite surface for enhanced mechanical properties and flame retardant behaviors. *ACS Appl. Mater. Interfaces* **2014**, *6*, 7223−7235.

(7) Hou, Y.; Hu, W.; Liu, L.; Gui, Z.; Hu, Y. In-situ synthesized CNTs/Bi_2Se_3 nanocomposites by a facile wet chemical method and its application for enhancing fire safety of epoxy resin. *Compos. Sci. Technol.* **2018**, *157*, 185−194.

(8) Yu, B.; Tawiah, B.; Wang, L.-Q.; Yuen, A. C. Y.; Zhang, Z.-C.; Shen, L.-L.; Lin, B.; Fei, B.; Yang, W.; Li, A.; Zhu, S.-E.; Hu, E.-Z.; Lu, H.-D.; Yeoh, G. H. Interface decoration of exfoliated MXene ultra-thin nanosheets for fire and smoke suppressions of thermoplastic polyurethane elastomer. *J. Hazard. Mater.* **2019**, *374*, 110−119.

(9) Malkappa, K.; Ray, S. S.; Kumar, N. Enhanced thermo-mechanical stiffness, thermal stability, and fire retardant performance of surface-modified 2D MoS_2 nanosheet-reinforced polyurethane composites. *Macromol. Mater. Eng.* **2019**, *304*, 1800562.

(10) Wang, J.; Yuan, B.; Cai, W.; Qiu, S.; Tai, Q.; Yang, H.; Hu, Y. Facile design of transition metal based organophosphorus hybrids towards the flame retardancy reinforcement and toxic effluent elimination of polystyrene. *Mater. Chem. Phys.* **2018**, *214*, 209−220.

(11) Xiao, H.; Liu, S. Zirconium phosphate (ZrP)-based functional materials: Synthesis, properties and applications. *Mater. Des.* **2018**, *155*, 19−35.

(12) Jiang, T.; Liu, C.; Liu, L.; Hong, J.; Dong, M.; Deng, X. Synergistic flame retardant properties of a layered double hydroxide in combination with zirconium phosphonate in polypropylene. *RSC Adv.* **2016**, *6*, 91720−91727.

(13) Yang, Y.; Liu, C.; Wu, H. Preparation and properties of poly (vinyl alcohol)/exfoliated α-zirconium phosphate nanocomposite films. *Polym. Test.* **2009**, *28*, 371−377.

(14) Clearfield, A.; Stynes, J. A. The preparation of crystalline zirconium phosphate and some observations on its ion exchange behaviour. *J. Inorg. Nucl. Chem.* **1964**, *26*, 117−129.

(15) Lu, H.; Wilkie, C. A. The influence of α-zirconium phosphate on fire performance of EVA and PS composites. *Polym. Adv. Technol.* **2011**, *22*, 1123−1130.

(16) Wang, X.; Zhao, D.; Medina, I. B. N.; Diaz, A.; Wang, H.; Clearfield, A.; Mannan, M. S.; Cheng, Z. Surface modification of layered zirconium phosphate with PNIPAM. *Chem. Commun.* **2016**, *52*, 4832−4835.

(17) Kalita, H.; Kumar, B. N. P.; Konar, S.; Tantubay, S.; Mahto, M. K.; Mandal, M.; Pathak, A. Sonochemically synthesized biocompatible zirconium phosphate nanoparticles for pH sensitive drug delivery application. *Mater. Sci. Eng., C* **2016**, *60*, 84−91.

(18) Xie, H.; Lai, X.; Li, H.; Zeng, X. Fabrication of ZrP nanosheet decorated macromolecular charring agent and its efficient synergism with ammonium polyphosphate in flame-retarding polypropylene. *Composites, Part A* **2018**, *105*, 223−234.
(19) Fei, G.; Liu, Y.; Wang, Q. Synergistic effects of novolac-based char former with magnesium hydroxide in flame retardant polyamide-6. *Polym. Degrad. Stab.* **2008**, *93*, 1351−1356.
(20) Malkappa, K.; Ray, S. S. Thermal stability, pyrolysis behavior, and fire-retardant performance of melamine cyanurate@poly-(cyclotriphosphazene-co-4, 4′-sulfonyl diphenol) hybrid nanosheet-containing polyamide 6 composites. *ACS Omega* **2019**, *4*, 9615−9628.
(21) Dabrowski, F.; Bourbigot, S.; Delobel, R.; Le Bras, M. Kinetic modelling of the thermal degradation of polyamide-6 nanocomposite. *Eur. Polym. J.* **2000**, *36*, 273−284.
(22) Xiang, H.; Li, L.; Chen, W.; Yu, S.; Sun, B.; Zhu, M. Flame retardancy of polyamide 6 hybrid fibers: Combined effects of α-zirconium phosphate and ammonium sulfamate. *Prog. Nat. Sci.: Mater. Int.* **2017**, *27*, 369−373.
(23) Xu, W.; Wang, X.; Wang, G.; Li, A.; Xu, B. A novel graphene hybrid for reducing fire hazard of epoxy resin. *Polym. Adv. Technol.* **2018**, *29*, 1194−1205.
(24) Xing, W.; Zhang, P.; Song, L.; Wang, X.; Hu, Y. Effects of alpha-zirconium phosphate on thermal degradation and flame retardancy of transparent intumescent fire protective coating. *Mater. Res. Bull.* **2014**, *49*, 1−6.
(25) Xiao, Y.; Xu, J.; Huang, S.; Deng, H. Effects of α-ZrP on crystallinity and flame-retardant behaviors of PA6/MCA composites. *Int. J. Polym. Sci.* **2017**, *2017*, 6034741.
(26) Liu, W.; Huang, X.; Wei, H.; Tang, X.; Zhu, L. Intrinsically fluorescent nanoparticles with excellent stability based on a highly crosslinked organic−inorganic hybrid polyphosphazene material. *Chem. Commun.* **2011**, *47*, 11447−11449.
(27) Ozay, H.; Ozay, O. Synthesis and characterization of drug microspheres containing phosphazene for biomedical applications. *Colloids Surf., A* **2014**, *450*, 99−105.
(28) Liu, W.; Zheng, Y.; Li, J.; Liu, L.; Huang, X.; Zhang, J.; Kang, X.; Tang, X. Novel polyurethane networks based on hybrid inorganic/organic phosphazene-containing nanotubes with surface active hydroxyl groups. *Polym. Adv. Technol.* **2012**, *23*, 1−7.
(29) Carroll, A. P.; Shaw, R. A. Phosphorus-nitrogen compounds. Part XXI. Alkylthio- and phenylthio-cyclotriphosphazatrienes. *J. Chem. Soc. A* **1966**, 914−921.
(30) Wei, W.; Huang, X.; Chen, K.; Tao, Y.; Tang, X. Fluorescent organic−inorganic hybrid polyphosphazene microspheres for the trace detection of nitroaromatic explosives. *RSC Adv.* **2012**, *2*, 3765−3771.
(31) Köhler, J.; Kühl, S.; Keul, H.; Möller, M.; Pich, A. Synthesis and characterization of polyamine-based cyclophosphazene hybrid microspheres. *J. Polym. Sci., Part A: Polym. Chem.* **2014**, *52*, 527−536.
(32) Tan, Y.; Shao, Z.-B.; Chen, X.-F.; Long, J.-W.; Chen, L.; Wang, Y.-Z. Novel multifunctional organic−inorganic hybrid curing agent with high flame-retardant efficiency for epoxy resin. *ACS Appl. Mater. Interfaces* **2015**, *7*, 17919−17928.
(33) Tan, Y.; Shao, Z.-B.; Yu, L.-X.; Long, J.-W.; Qi, M.; Chen, L.; Wang, Y.-Z. Piperazine-modified ammonium polyphosphate as monocomponent flame-retardant hardener for epoxy resin: flame retardance, curing behavior and mechanical property. *Polym. Chem.* **2016**, *7*, 3003−3012.
(34) Tan, Y.; Shao, Z.-B.; Yu, L.-X.; Xu, Y.-J.; Rao, W.-H.; Chen, L.; Wang, Y.-Z. Polyethyleneimine modified ammonium polyphosphate toward polyamine-hardener for epoxy resin: thermal stability, flame retardance and smoke suppression. *Polym. Degrad. Stab.* **2016**, *131*, 62−70.
(35) Sun, L.; Boo, W. J.; Sue, H.-J.; Clearfield, A. Preparation of α-zirconium phosphate nanoplatelets with wide variations in aspect ratios. *New J. Chem.* **2007**, *31*, 39−43.
(36) Liu, X.-Q.; Wang, D.-Y.; Wang, X.-L.; Chen, L.; Wang, Y.-Z. Synthesis of functionalized α-zirconium phosphate modified with intumescent flame retardant and its application in poly (lactic acid). *Polym. Degrad. Stab.* **2013**, *98*, 1731−1737.
(37) Qiu, S.; Ma, C.; Wang, X.; Zhou, X.; Feng, X.; Yuen, R. K. K.; Hu, Y. Melamine-containing polyphosphazene wrapped ammonium polyphosphate: A novel multifunctional organic-inorganic hybrid flame retardant. *J. Hazard. Mater.* **2018**, *344*, 839−848.
(38) Mosby, B. M.; Díaz, A.; Bakhmutov, V.; Clearfield, A. Surface functionalization of zirconium phosphate nanoplatelets for the design of polymer fillers. *ACS Appl. Mater. Interfaces* **2013**, *6*, 585−592.
(39) Fu, Y.; Teng, Y.; Yu, G.; Yin, C. Synthesis and structure properties of flame retardant and cationic dyeable polyamide 6 modified with 5-sulfoisophthalic acid sodium and melamine cyanurate. *Fibers Polym.* **2018**, *19*, 1363−1372.
(40) Xu, L.; Lei, C.; Xu, R.; Zhang, X.; Xu, J. Intumescent flame retardant of polypropylene system with enhanced thermal properties and flame retardancy based on α-zirconium phosphate composite particles. *Polym. Bull.* **2018**, *75*, 2707−2727.
(41) Tajvidi, M.; Falk, R. H.; Hermanson, J. C. Effect of natural fibers on thermal and mechanical properties of natural fiber polypropylene composites studied by dynamic mechanical analysis. *J. Appl. Polym. Sci.* **2006**, *101*, 4341−4349.
(42) Illers, V. K.-H. Der Einfluß von Wasser auf die molekularen Beweglichkeiten von Polyamiden. *Die Makromolekulare Chem.* **1960**, *38*, 168−188.
(43) Owen, A. J.; Ward, I. M. Mechanical anisotropy in nylon 6 and nylon 6.6. *J. Macromol. Sci., Part B: Phys.* **1973**, *7*, 279−296.
(44) Gadekar, R.; Kulkarni, A.; Jog, J. P. Blends of nylon with polyethylene: Effect of compatibilization on mechanical and dynamic mechanical properties. *J. Appl. Polym. Sci.* **1998**, *69*, 161−168.
(45) Kolařík, J.; Janáček, J. Secondary (β) relaxation process of alkaline polycaprolactam swollen by low molecular weight substances. *J. Polym. Sci., C Polym. Symp.* **1967**, *16*, 441−449.
(46) Awad, W. H.; Wilkie, C. A. Investigation of the thermal degradation of polyurea: the effect of ammonium polyphosphate and expandable graphite. *Polymer* **2010**, *51*, 2277−2285.
(47) Singh, S.; Wu, C.; Williams, P. T. Pyrolysis of waste materials using TGA-MS and TGA-FTIR as complementary characterisation techniques. *J. Anal. Appl. Pyrolysis* **2012**, *94*, 99−107.
(48) Dong, Y.; Gui, Z.; Hu, Y.; Wu, Y.; Jiang, S. The influence of titanate nanotube on the improved thermal properties and the smoke suppression in poly (methyl methacrylate). *J. Hazard. Mater.* **2012**, *209-210*, 34−39.
(49) Jiang, S.-D.; Bai, Z.-M.; Tang, G.; Song, L.; Stec, A. A.; Hull, T. R.; Zhan, J.; Hu, Y. Fabrication of Ce-doped MnO_2 decorated graphene sheets for fire safety applications of epoxy composites: flame retardancy, smoke suppression and mechanism. *J. Mater. Chem. A* **2014**, *2*, 17341−17351.
(50) Jiang, S.-D.; Tang, G.; Chen, J.; Huang, Z.-Q.; Hu, Y. Biobased polyelectrolyte multilayer-coated hollow mesoporous silica as a green flame retardant for epoxy resin. *J. Hazard. Mater.* **2018**, *342*, 689−697.

https://dx.doi.org/10.1021/acsomega.0c01247
ACS Omega 2020, 5, 13867−13877